Z. Phys. C – Particles and Fields 43, 1–14 (1989)

Zeitschrift für Physik C Particles and Fields

An experimental study of e^+e^- annihilation into four leptons at $\sqrt{S} \geqq 35$ GeV

CELLO Collaboration

H.-J. Behrend, L. Criegee, J.B. Dainton[1], J.H. Field[2], G. Franke, H. Jung[3], J. Meyer, V. Schröder, G.G. Winter
Deutsches Elektronen-Synchrotron, DESY, D-2000 Hamburg, Federal Republic of Germany

P.J. Bussey, C. Buttar[4], A.J. Campbell, D. Hendry, G. McCurrach, J.M. Scarr, I.O. Skillicorn, K.M. Smith
University of Glasgow, Glasgow G12 8QQ, UK

J. Ahme, V. Blobel, W. Brehm, M. Feindt, H. Fenner, J. Harjes, J.H. Peters, O. Podobrin, H. Spitzer
II. Institut für Experimentalphysik, Universität Hamburg, D-2000 Hamburg, Federal Republic of Germany

W.-D. Apel, J. Engler, G. Flügge[3], D.C. Fries, J. Fuster[5], P. Gabriel, K. Gamerdinger[6], P. Grosse-Wiesmann[7], M. Hahn, U. Hädinger, J. Hansmeyer, H. Küster[8], H. Müller, K.H. Ranitzsch, H. Schneider, R. Seufert
Kernforschungszentrum Karlsruhe und Universität Karlsruhe, D-7500 Karlsruhe, Federal Republic of Germany

W. de Boer, G. Buschhorn, G. Grindhammer[7], B. Gunderson, Ch. Kiesling[9], R. Kotthaus, H. Kroha, D. Lüers, H. Oberlack, P. Schacht, S. Scholz, G. Shooshtari[10], W. Wiedenmann
Max-Planck-Institut für Physik und Astrophysik, D-8000 München, Federal Republic Germany

M. Davier, D. Fournier, J.F. Grivaz, J. Haïssinski, P. Janot, V. Journé, D.W. Kim, F. Le Diberder, J.-J. Veillet
Laboratoire de l'Accélérateur Linéaire, F-91405 Orsay Cedex, France

K. Blohm, R. George, M. Goldberg, O. Hamon, F. Kapusta, L. Poggioli, M. Rivoal
Laboratoire de Physique Nucléaire et des Hautes Energies, Université de Paris, F-75230 Paris Cedex, France

G. D'Agostini, F. Ferrarotto, M. Iacovacci, B. Stella
University of Rome and INFN, I-00185, Italy

R. Aleksan, G. Cozzika, Y. Ducros, F. Pierre
Centre d'Etudes Nucléaires, Saclay, F-91191 Gif-sur-Yvette, France

G. Alexander, A. Beck, G. Bella, J. Grunhaus, A. Klatchko, A. Levy, C. Milstène
Tel Aviv University, 69978 Ramat Aviv, Israel

Received 18 January 1989

Abstract. The three reactions $e^+e^- \to e^+e^-e^+e^-$, $e^+e^- \to e^+e^-\mu^+\mu^-$ and $e^+e^- \to \mu^+\mu^-\mu^+\mu^-$ have been studied using the CELLO detector at PETRA. The data correspond to 130 pb^{-1} collected at energies ranging from 35 GeV to 46.8 GeV. A detailed analysis of the distribution of the observed events in phase space shows good agreement with QED to order α^4.

1 Introduction

The study of higher order QED processes over as wide a range of kinematic conditions as possible provides an important test of the theory. Such investigations are best carried out at e^+e^- colliders, and require relatively high integrated luminosities. In this paper we report the results of a study carried out by the CELLO collaboration, of the α^4 reactions $e^+e^- \to e^+e^-e^+e^-$, $e^+e^- \to e^+e^-\mu^+\mu^-$ and $e^+e^- \to \mu^+\mu^-\mu^+\mu^-$, based on a total integrated luminosity of 130 pb^{-1} taken at $\sqrt{S} \geqq 35$ GeV. The aim of this

[1] Permanent address: University of Liverpool, UK
[2] Now at Université de Genève, Switzerland
[3] Now at RWTH, Aachen, FRG
[4] Now at Nuclear Physics Laboratory, Oxford, UK
[5] Now at Instituto de Fisica Corpuscular, Universidad de Valencia, Spain
[6] Now at MPI, München, FRG
[7] Now at SLAC, Stanford, USA
[8] Now at DESY, Hamburg, FRG
[9] Heisenberg-Stipendiat der Deutschen Forschungsgemeinschaft
[10] Now at University of Rome, Italy

analysis is to bring out dynamical effects not studied in previous experiments [1]. For example, in the so-called single-tag configuration, the comparison of our data with an analytical expression for the complete differential cross section provides the first evidence for several *large* effects such as azimuthal correlations and charge asymmetries.

To examine the global features of the cross section, the one-dimensional distributions of various kinematical variables are usually compared with the QED predictions. However, due to the intricate kinematics and dynamics of the processes under consideration, such distributions do not provide clear evidence for the presence of the individual terms contributing to the differential cross section. Thus we have been led to use extensively the maximum likelihood method, which provides an almost detector-independent measurement of the predicted charge symmetry violation.

2 QED predictions

2.1 Generalities

The lowest order Feynman diagrams which describe the reactions $e^+e^- \to 4$ leptons involve two virtual photons γ_1 and γ_2. These diagrams can be grouped in three (gauge invariant) sets in the following way:

a) the set G_{conv} (Fig. 1a) which contains the 'single conversion' diagrams involving one photon, γ_1, with a negative four-momentum squared, $P^2_{\gamma_1} < 0$, while the other has $P^2_{\gamma_2} > 0$,

b) the set G_{conv^2} (Fig. 1b) which contains the 'double conversion' diagrams with two timelike photons ($P^2_{\gamma_{1,2}} > 0$),

c) the set G_{mul} (Fig. 1c) which contains the 'multiperipheral' diagrams with two spacelike photons ($P^2_{\gamma_{1,2}} < 0$). These are the conventional 'photon-photon interaction' diagrams.

The relative importance of the three groups strongly depends on the region of phase space considered and on the final state under study (see Table 1), We refer to final states as single-tag or double-tag according to whether one or two high energy electrons or positrons emerge at large angles to the beam direction. For convenience, the final state configuration with four muons produced at large angle is also referred to as the double-tag configuration. For the study of double-tag processes, we have used the Monte-Carlo generator described in [2].

2.2 The single-tag configuration

Large simplifications occur for reactions $ee \to eeff$ ($f = e, \mu, \tau, u, d \ldots$) in the kinematical configuration where the final state positron (or electron) is scattered

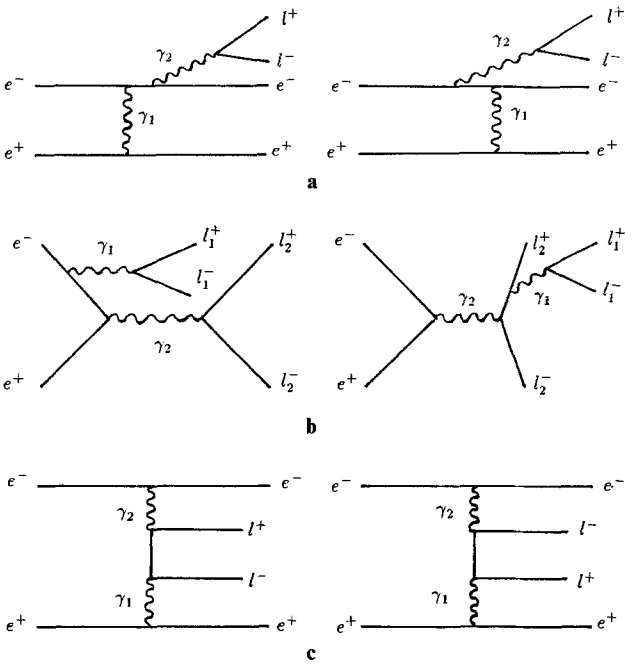

Fig. 1a–c. Examples of Feynman diagrams corresponding to the three groups G_{conv}, G_{conv^2} and G_{mul}

Table 1. Numbers of diagrams involved in the different groups for the three final states considered in the analysis. Numbers in parenthesis correspond to the single-tag configuration

	G_{conv}	G_{conv^2}	G_{mul}	Total
$ee\mu\mu$	4 (2)	6 (0)	2 (2)	12 (4)
$eeee$	16 (4)	12 (0)	8 (4)	36 (8)
$\mu\mu\mu\mu$	0 (0)	12 (0)	0 (0)	12 (0)

at a small angle. In the following, for the sake of definiteness, the small angle particle will be assumed to be a positron labelled (e^+), while the electron scattered at larger angle will be noted [e^-]. Reactions involving an electron (e^-) produced at a small angle and a tagged positron [e^+] are related to the previous ones by a CP transformation.

To a very good approximation, such events can be described by retaining only those diagrams which involve a quasi-real photon γ_1 attached to the (e^+) leg as shown in Fig. 2. The numbers of diagrams to be taken into account are given in Table 1. In addition, after integration over the azimuthal angle of the positron (e^+) (which is experimentally badly defined

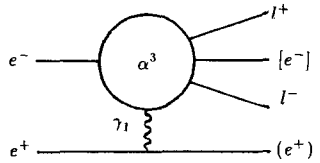

Fig. 2. Structure of the main diagrams in the single-tag configuration

being usually unmeasured), the differential cross section of the α^4 reaction, $d\sigma_4$, can be factorized into two terms. The first, $d\sigma_1$, describes the order α reaction $e^+ \to (e^+)\gamma_1$ while the second, $d\sigma_3$, describes the order α^3 reaction $\gamma_1 e^- \to [e^-] l^+ l^-$. We obtain:

$$d\sigma_4 = d\sigma_1 \, d\sigma_3,$$

with

$$d\sigma_1 = \frac{\alpha}{\pi}\frac{dg^2}{g^2}\frac{dk}{k}\left(1-k+\frac{k^2}{2}-(1-k)\frac{g^2_{\min}}{g^2}\right), \quad (1)$$

where

- $g^2 = -(P_{e^+} - P_{(e^+)})^2 = -P^2_{\gamma_1}$,
- $k = \dfrac{E_{\gamma_1}}{E_b}$ is the fraction of the beam energy E_b taken by the photon γ_1,
- $g^2_{\min} = m_e^2 \dfrac{k^2}{1-k}$ is the minimum value of g^2.

Usually the differential cross section $d\sigma_3$ receives its main contribution from the two multiperipheral diagrams common to both the $ee\mu\mu$ and $eeee$ final states (see Fig. 1c). In the single-tag configuration, these diagrams (referred to as leading diagrams in the following) may be viewed as describing the deep inelastic scattering of an electron off the quasi real photon γ_1. Thus $d\sigma_3$ is most naturally expressed in terms of the standard scaling variables used in deep inelastic scattering:

$$x = \frac{Q^2}{Q^2+W^2},$$
$$y = 1-(1-K)\cos^2\frac{\theta_{[e^-]}}{2}, \quad (2)$$

where

- $Q^2 = -P^2_{\gamma^*}$ (here $P_{\gamma^*} = P_{e^-} - P_{[e^-]}$ is the 4-momentum of the virtual photon γ^* exchanged in the deep inelastic process)
- $W^2 = (P_{l^-} + P_{l^+})^2$ is the invariant mass squared of the two leptons,
- $K = \dfrac{E_{\gamma^*}}{E_b}$ is the fraction of the beam energy taken by γ^*,
- $\theta_{[e^-]}$ is the scattering angle of the $[e^-]$ electron with respect to the direction of the electron beam.

In the centre-of-mass of the two produced leptons the z axis is taken along the γ_1 direction while the azimuthal angles are defined with respect to the transverse direction of the electron $[e^-]$. Let θ^-_* and ϕ^-_* be the polar and azimuthal angles of the l^- lepton in that frame. By crossing the known matrix elements [3] for the processes $e^+e^- \to \gamma l^+ l^-$ ($l = e, \mu$) we obtain:

$$\frac{d\sigma_3}{dx\,dy\,d\cos\theta^-_*\,d\phi^-_*} = \frac{\alpha^3}{E_b^2\,k\,x^2}\Delta_{\text{mul}} \times \Delta_{\text{conv}} \times \Delta_{\leftrightarrow}, \quad (3)$$

where the three (dimensionless) factors have the following meaning:

The two first terms Δ_{mul} and Δ_{conv} correspond respectively to the contribution of the 2 leading diagrams and to the correction introduced by the 2 single conversion diagrams common to both the $ee\mu\mu$ and the $eeee$ final states (Fig. 1a). The third term, $\Delta_{\leftrightarrow}$, specific to the $eeee$ final state, accounts for the 4 diagrams related to the 4 previous ones by the exchange $l^- \leftrightarrow [e^-]$.

The multiperipheral contribution may be expressed as follows:

$$\Delta_{\text{mul}} = f_0(y)(2xF_\perp) + f_1(y)(F_\parallel + \cos 2\phi^-_* F^\perp_\perp) - f_2(y)(\cos\phi^-_* F^\parallel_\perp) \quad (4)$$

where the functions $f_{0,1,2}$ are related to the polarization matrix of the photon γ_2 which, in the diagrams of Fig. 1c, may be identified with γ^*. Their expressions are:

$$f_0(y) = \frac{4}{y^2}\left(1-y+\frac{y^2}{2}\right), \quad f_1(y) = \frac{4}{y^2}(1-y)$$
and
$$f_2(y) = \frac{2}{y^2}(2-y)\sqrt{1-y}. \quad (5)$$

The four 'structure functions' $F_\perp, F_\parallel, F^\perp_\perp$ and $F^\parallel_\perp$ are given by*

$$F_\perp(x,z) = \frac{1}{8}(x^2+(1-x)^2)\frac{1+z^2}{1-z^2},$$
$$F_\parallel(x,z) = x^2(1-x),$$
$$F^\perp_\perp(x,z) = \frac{x^2}{2}(1-x), \quad (6)$$
$$F^\parallel_\perp(x,z) = x(1-2x)\,z\sqrt{\frac{x(1-x)}{1-z^2}},$$

where the z variable is defined by

$$z = \cos\theta^-_* \sqrt{\left(1-\frac{g^2 x}{2E_b^2 k y}\right)\left(1-\frac{4m_l^2}{W^2}\right)}.$$

* Eqs. (6) hold for $\cos^2\theta^-_*$ not too close to 1. More complete formulae may be found in [4]

The 'single conversion' correction term takes the simple form:

$$\Delta_{\text{conv}} = 1 + \delta^2 + 2\delta \cos \phi_*^-$$

where

$$\delta = \frac{y}{2} \sqrt{\frac{x(1-z^2)}{(1-x)(1-y)}}. \tag{7}$$

Finally the correction term specific to the $eeee$ final state is given by

$$\Delta_{\leftrightarrow} = 1 + \frac{(uu_* - tt_*)(u^2+u_*^2) + ss_*(s^2+s_*^2)}{tt_*(t^2+t_*^2+u^2+u_*^2)},$$

where

$$\begin{aligned} s &= -2xy, \\ s_* &= 2y(1-x), \\ t &= -(1-xy+v), \\ t_* &= (1-y+xy+(yz-v)), \\ u &= -(1-xy-v), \\ u_* &= (1-y+xy-(yz-v)), \\ v &= z(1-x(2-y)) - 2\sqrt{x(1-x)(1-y)(1-z^2)} \cos \phi_*^-. \end{aligned} \tag{8}$$

The relative complexity of this last expression arises from the fact that $\Delta_{\leftrightarrow}$ restores the invariance of $d\sigma_3$ under the transformation $l^- \leftrightarrow [e^-]$ which is broken in Δ_{mul}.

None of the terms discussed above may be safely neglected when dealing with the full differential cross section. It is only in the 'no-tag' case, when γ^* and γ_1 are both quasi-real ($x \ll 1$), that one can drop all terms except the $F_\perp$ contribution to Δ_{mul}. When considering the $ee\mu\mu$ final state, although from expressions (4) and (7) one may expect to have to retain only the $F_\perp$ and $F_\parallel$ contributions after integration over ϕ_*^-, such an approximation is not valid. This is because a simple acceptance cut, such as $|\cos \theta_{l^\pm}| < \cos_{\max}$ defined in the laboratory frame, translates into an acceptance which depends strongly on ϕ_*^- in the $l^+ l^-$ centre-of-mass, and prevents the self-cancellation on the average of the contribution of terms such as $F_\perp^\parallel$.

For the study of the single-tag processes, we have used a Monte-Carlo simulation based on (1) and (3), in which the differential cross section is written as:

$$d\sigma_4 = d\sigma_1 \, d\sigma_3 \times \Delta_{\alpha^4}.$$

The fourth correction term, Δ_{α^4}, in contrast with Δ_{conv} and $\Delta_{\leftrightarrow}$, is very close to unity. It is deduced from the exact α^4-expression for the matrix element squared of the process given in [5] and available in the Monte-Carlo program described in [2]. It corrects for the approximations made in the treatment of the non-vanishing values of g^2, m_e^2 and m_l^2 in the formulae given above, for the approximations involved in the factorization $d\sigma_4 = d\sigma_1 \, d\sigma_3$, and for the omitted diagrams. Its presence ensures that the expression of $d\sigma_4$ used in the Monte-Carlo simulation of the process is exact to order α^4.

2.3 Radiative corrections

To account for small corrections induced by the possible emission of photons from the leptonic lines we have used an equivalent radiator method. To describe the production of photons at small angles we used a formula similar to expression (1) which neglects the contribution of the final state leptons. For isolated photons which are emitted at large angles with respect to both initial and final state particles, such as those considered in Section 5.3, the contributions of all six lepton lines and their interferences have been included in a separate Monte-Carlo program based on results given in [6].

3 The experiment

The data were taken with the CELLO detector at PETRA at centre-of-mass energies between 35 and 46.8 GeV. The total integrated luminosity is 130 pb^{-1}.

3.1 The CELLO detector

CELLO [7] is a general purpose magnetic detector equipped with a thin superconducting solenoid. The tracking system enables the detection of charged particles down to $|\cos \theta| < 0.976$. In the central region, $|\cos \theta| < 0.85$, 14 interleaved cylindrical drift and proportional chambers yield a momentum measurement with a resolution of $\sigma(p)/p = 1\% \, p$, p in GeV. The detection of electromagnetic showers is performed down to 50 mrad by a combination of four components. In the central region a cylindrical liquid argon calorimeter provides an energy measurement with a resolution of $\sigma(E)/E = 0.05 + 0.10/\sqrt{E}$, E in GeV. It is supplemented on both sides by two end-cap liquid argon calorimeters which provide a similar energy resolution in the angular range extending from 140 mrad to 350 mrad. The acceptance gap between the end-caps and the cylindrical calorimeter is covered with a lead scintillator sandwich. At small angle the acceptance is closed by two lead glass arrays (one on each side of the detector). From 50 mrad to 80 mrad, it

ensures an energy measurement with a resolution of $\sigma(E)/E = 12\%$ at high energy. Angular measurements are performed with resolutions which are typically better than 10 mrad. For charged-particle identification the fine grain liquid argon calorimeter is used. In addition, muons are detected behind an 80 cm thick iron absorber by planar drift chambers covering 92% of 4π.

In this analysis, events are classified according to the detector components which detected the electrons. The forward detector, the end-caps and the cylindrical part of the liquid argon calorimeter will be denoted as *FW*, *EC* and *CY*, respectively.

3.2 *Preselection*

A remarkable feature of final states involving up to four particles is that the knowledge of the particle directions is by itself sufficient to determine their energies. The angular measurement being usually of very good quality for charged particles, such a determination leads to a precise reconstruction of the kinematics. Once completed by a true kinematical fit which takes into account the energy measurements and which allows for the possible presence of additional photons, this procedure ends with an almost perfect reconstruction of the final state kinematics.

In order to merge in a simple way different data sets taken at various centre-of-mass energies, the preselection as well as the final selection and the analysis should not depend on the beam energy. For this reason the preselection was done in the following way:

- On the basis of the detector measurements and making use of loose and scale invariant cuts, four-lepton events are selected together with certain other kinds of events such as those produced by the α^3 QED reaction $e^+e^- \to e^+e^-\gamma$.
- All selected events are submitted to a kinematical fit which in particular allows for the omission of badly measured energy. The events produced by the α^3 QED reaction mentioned above are used to study the detector performances (in particular those of the tagging devices), to define some 'good fit' criteria and to determine the integrated luminosity. The total integrated luminosity used is found to be equivalent to 160 pb^{-1} taken at a fixed centre-of-mass energy of 40 GeV.
- Only those events leading to a 'good fit' are then retained for the subsequent analysis in which only *fitted* and *scaled* – hence dimensionless – quantities are considered. For example, in the following, the momentum p of a given particle appears only in its ratio to the beam energy $r = p/E_b$. Accordingly, most of the quoted numbers below are given without units.

3.3 *Particle identification*

Charged particles are classified as to whether they are fully identified or simply compatible with a given lepton flavour hypothesis. Only the most important identification criteria are discussed, more details can be found in [4].

3.3.a Muon identification. The identification of a particle as a muon is limited to the region $|\cos\theta| < 0.92$. A good correlation between the hit associated to the track in a muon chamber and its expected impact is required and in addition, an energy deposition in the calorimeter compatible with that expected from a minimum ionizing particle. If only the second condition is met, the particle is considered to be compatible with the muon hypothesis. The overall identification efficiency as determined from the data is of the form:

$$\varepsilon_\mu \simeq 0.78\left(1-\exp\left(-\left(\frac{rE_b-1}{0.6}\right)^2\right)\right), \text{ with } E_b \text{ in GeV.}$$

In order to reduce the scale-invariance breaking effect induced by the E_b dependence of ε_μ, the muon identification is limited in the present analysis to particles with $r > 0.10$.

3.3.b Electron identification. For a particle to be fully identified as an electron, its track is required to satisfy $0.05 < |\cos\theta| < 0.85$ and $r > 0.05$, plus further criteria concerning the characteristic shower development expected for an electromagnetic shower and the compatibility between the energy measured in the calorimeter and the momentum measured with the central chambers. The overall identification efficiency as obtained from the data is 94% and is almost independent of E_b. In the angular domain covered by the tracking system ($|\cos\theta| < 0.976$) a charged particle is considered to be compatible with the electron hypothesis if it is not compatible with the muon hypothesis and if its associated shower does not exhibit the late development characteristic of a hadron.

3.3.c Lepton pair identification. To be identified as a lepton pair, two particles l_1 and l_2 must satisfy the following criteria:

- both particles must have a (scaled) transverse momentum above 0.015 and must originate from the interaction vertex,
- at least one particle must be identified as an electron or a muon, while the other must be a lepton of the same flavour but with opposite charge, or at least must be compatible with such a hypothesis.

In addition, to ensure the scale invariance of the analysis, the invariant mass of the two particles must satisfy $W_{l^+l^-} > 0.05$ (0.01) for a pair of muons (elec-

trons). Furthermore, in the case of electrons, the pair must satisfy one of the following conditions:

- $|\theta_{t_1} - \theta_{t_2}| > 2°$, where $\theta_{t_{1,2}}$ are the polar angles of the two tracks,
- $L_{bp} > 2$ cm, where L_{bp} is the distance between the points of intersection of the tracks with the beam-pipe.

If an electron pair does not satisfy any of the two latter conditions it is assumed to result from the conversion of a photon in the beam pipe. If the pair satisfies only one condition it is considered to be compatible with a converted photon.

3.3.d Isolated particle. Any particle (charged or neutral) is defined to be isolated if it satisfies the three following conditions:

- $|\cos\theta| < 0.99$,
- $r > 0.05$,
- $\psi_{min} > 10°$, where ψ_{min} is the minimal opening angle between its direction and the directions of other charged particles.

4 Analysis of the single-tag events

Following the convention introduced in Sect. 2.2, the following discussion of single-tag events refers to events where the antitagged particle (e^+) is scattered at small angle with respect to the direction of the positron beam. Events where this particle escapes detection in the direction of the electron beam are submitted to a CP transformation and are then analysed as described below.

4.1 Event selection

The selection isolates events with:

- 1 tagged electron $[e^-]$.
- 1 anti-tagged particle (e^+) which is assumed to be the positron and must satisfy $\pi - \theta_{(e^+)} < 50$ mrad and $r_{(e^+)} > 0.025$. Although this particle is usually undetected, its momentum is available, being reconstructed in the fitting procedure.
- 2 particles identified as a lepton pair, both detected within $|\cos\theta| < 0.92$ and at least one within $|\cos\theta| < 0.85$.
- no isolated photon.

The events enter into six classes FW^l, EC^l and CY^l ($l = e, \mu$) depending on the lepton pair type l and on the detector component where the $[e^-]$ is detected. Additional acceptance cuts are listed below. All the CY events and a selection of the FW and EC events have been visually inspected.

4.1.a FW and EC tag events. A particle is identified as a FW (EC) tag electron if it satisfies $r_{[e^-]} > 0.5$ and 55 mrad $< \theta_{[e^-]} <$ 75 mrad (150 mrad $< \theta_{[e^-]} <$ 350 mrad). To reduce the background from double radiative events (see Sect. 4.2), the anti-tagged positron must also satisfy $r_{(e^+)} > 0.5$. In order to restrict the analysis to a phase space domain where the experimental acceptance is smooth, both particles of the l^+l^- pair must satisfy $|\cos\theta| < 0.85$ and at least one must have a transverse momentum above 0.04. In addition, in the case of the $eeee$ final state, the l^+l^- pair must not be compatible with the converted photon hypothesis (cf. Sect. 3.3.c).

4.1.b CY tag events. Three charged particles within $|\cos\theta| < 0.92$ are required. Among them at least one must have a negative charge and be identified as an electron, while the two other ones must form a lepton pair. In the $eeee$ final state, the $[e^-]$ tag is defined to be the electron with the highest energy and both l^+l^- and $l^+[e^-]$ pairs must have invariant masses above 0.01, none of them being compatible with a converted photon.

4.2 Background

Due to the requirements of a 'good fit', the lepton pair identification and, in the case of $eeee$ events, the rejection of events where the l^+l^- pair satisfies the loose criteria of compatibility with a converted photon hypothesis, only one potential source of background remains: The double radiative reaction $e^+e^- \to l^+l^-\gamma\gamma$. This reaction can fake four-lepton events if one of the photons, escaping detection at small angle, is assumed to be a positron (e^+) while the second photon is detected in the FW or EC calorimeter and considered as a tagged electron $[e^-]$. According to a Monte-Carlo simulation of the process (which makes use of an approximation similar to that discussed in Sect. 2.2) the main contribution appears in the EC^e class, where it accounts for 5% of the total number of events. In the analysis of the four classes FW^l and EC^l ($l = e, \mu$) the contribution from the double radiative process has been added to the four-lepton QED prediction.

4.3 Yields and kinematical distributions

The number of events observed in each of the six classes (cf. Table 2) and the experimental distributions of the kinematical variables show a good agreement with the QED predictions. A sample of distributions is presented in Fig. 3a to f. The complete set of distributions investigated may be found in [4]. The average (scaled) Q^2 values in the FW^l, EC^l and CY^l distributions are close to $4\cdot10^{-3}$ (Fig. 3a), $4\cdot10^{-2}$ and $4\cdot10^{-1}$ respectively. The Q^2 range covered by this analysis extends from 0.5 GeV^2 to $2\cdot10^3$ GeV^2. The double structure observed in the distribution of k (Fig. 3b) results from the combined effects of the dynamics, which favours the domains $k\ll1$ and $K\ll1$, and of the cut $r_\mu>0.10$ (cf. Sect. 3.3.a). This implies $k+K>0.10$ with either $k\sim0.10$ or $K\sim0.10$. Whereas, in the FW^l classes, the single conversion diagrams contribution, Δ_{conv}, is not sizeable in such distributions, this is no longer the case in the EC^e class. For instance, the distribution of x (Fig. 3c) in the region $x\simeq1$ cannot be accounted for with $\Delta_{\text{conv}}=1$. In the EC^μ class, due to the higher W cut ($W_{\mu^+\mu^-}>0.05$ instead of 0.01) the Δ_{conv} term plays a less pronounced rôle. For instance, no correction is needed to describe the W distribution (Fig. 3d). In the CY^e and CY^μ classes the contributions from the single conversion diagrams are large. These account for 24% and 32% respectively of the total cross sections. The effect of the non-leading diagrams is most easily observed through their interferences with the leading ones, in distributions of quantities involving the charge of the produced leptons such as ϕ_*^- and $\cos\theta_*^-$. The two leading diagrams, which have a definite $C_{l^+l^-}$ parity, lead to distributions which are invariant under the transformation $l^+\leftrightarrow l^-$. For example, they cannot account for the distribution of $|\phi_*^-|$ in the CY^e class (Fig. 3e) which, clearly, is not invariant under the transformation $|\phi_*^-|\leftrightarrow\pi-|\phi_*^-|$. Although less important, the effect is still apparent in Fig. 3f which displays the $\cos\theta_*^-$ distribution for the CY^μ class.

Table 2. Numbers of observed events in the single-tag configuration together with the corresponding QED predictions

	Observed	Predicted
FW^e	2120	2130 ± 62
EC^e	1115	1090 ± 40
CY^e	123	110 ± 11
FW^μ	563	550 ± 26
EC^μ	777	760 ± 31
CY^μ	75	77 ± 09

4.4 Analysis of the multiperipheral contribution

The combined effect of the acceptance cuts and of the non-leading diagrams is quite large. However, in the FW and EC classes where the statistics is high, the structure of the leading term Δ_{mul} can be analysed if one takes into account the full correlation between the four kinematical variables needed to describe the $e\gamma\to ell$ reaction. Such an analysis has been carried out, making use only of the normalized distribution of events in phase space, in the following way.

Owing to (4) the Δ_{mul} term can naturally be split in the form

$$\Delta_{\text{mul}}=(\alpha_0 H_0+\alpha_1 H_1+\alpha_2 H_2),$$

where the α_i are three constants, in principle equal to $+1$, and the H_i are three functions of the kinematical variables whose sum reproduces Δ_{mul}. We apply the likelihood method with an overall normalization constraint to determine the values to be given to the α parameters in order to describe the data in the best way. One expects $\alpha_i=+1$ if and only if the contributions to the total cross section of the functions H_i are precisely the same in the theoretical expression for σ and in the data, i.e. if the following equalities are satisfied:

$$\frac{\sigma_i^{\text{tot}}}{\sigma^{\text{tot}}}=\frac{1}{N}\sum_{k=1}^{N}\frac{H_i(k)}{\Delta_{\text{mul}}(k)}\qquad(i=0,1,2),\tag{9}$$

where

- σ_i^{tot} is the total cross section obtained when setting all the α parameters but α_i equal to 0,
- $H_i(k)$ and $\Delta_{\text{mul}}(k)$ denote the values taken by H_i and Δ_{mul} when the kinematical variables are those of the event number k.

Two decompositions of Δ_{mul} have been used. The main goal of the first is to analyse the y dependence of Δ_{mul}. It involves H_i functions of the form

$$F_i=f_i(y)\,\tilde{F}_i(x,\cos\theta_*^-,\phi_*^-),$$

where $f_i(y)$ $(i=0,1,2)$ are the three functions defined by (5). The aim of the second decomposition is to resolve the azimuthal correlations between the leptons and the $[e^-]$ electron in the l^+l^- centre-of-mass. It involves functions of the form

$$G_i=\cos(i\times\phi_*^-)\,\tilde{G}_i(x,y,\cos\theta_*^-).$$

Equation (4) gives for example $F_0=f_0(y)(2x\,F_\perp)$ and $G_2=\cos(2\times\phi_*^-)(f_1(y)\,F_\perp^\perp)$.

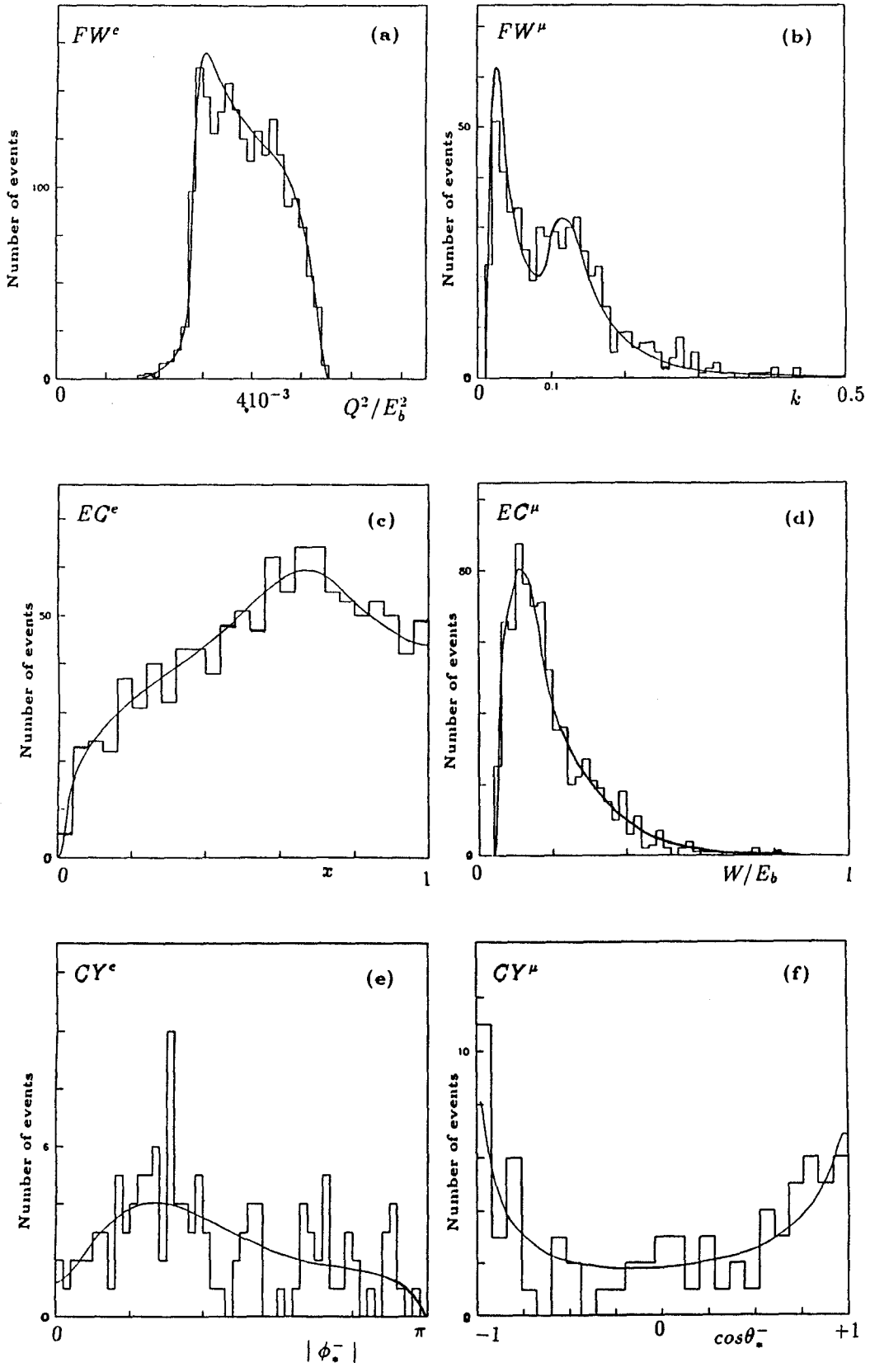

Fig. 3a–f. Sample of observed distributions (histograms) and the corresponding QED predictions normalized to the data (smooth curves) in the single-tag configuration. **a** Distribution of Q^2 in the FW^e class; **b** distribution of k in the FW^μ class; **c** distribution of x in the EC^e class; **d** distribution of W in the EC^μ class; **e** distribution of $|\phi_*^-|$ in the CY^e class; **f** distribution of $\cos\theta_*^-$ in the CY^μ class

The overall agreement between data and theory (9) is good (see Table 3). The contributions of the different terms of Δ_{mul} to the total cross section have been measured and found to be in good agreement with the QED prediction at the percent level.

Setting $\alpha_0 = 1$, the likelihood functions

$$L(\alpha_1, \alpha_2) = \prod_{k=1}^{N} \frac{\sum_0^2 \alpha_i H_i(k)}{\Delta_{\text{mul}}(k)} \frac{\sigma^{\text{tot}}}{\sum_0^2 \alpha_i \sigma_i^{\text{tot}}}$$

which, if (9) are exactly satisfied, may be identified with the confidence levels associated with a given hypothesis (α_1, α_2), peak sharply at values close to unity. The most stringent limits are obtained in the FW^e class where, for the first decomposition, one obtains $L(0,0) = 6 \cdot 10^{-40} L(1,1)$. The less stringent limits correspond to the FW^μ class, for the second decomposition, where, for example: $L(1,0) = 3 \cdot 10^{-3} L(1,1)$. In all four FW^l and EC^l classes and for both decompositions defined above, the data are inconsistent with setting any of the α_i equal to zero.

In the CY^l classes the contributions to the total cross section from the single conversion diagrams may be experimentally determined in a similar way from the distribution of the data in phase space. We thus obtain $(20 \pm 5)\%$ for the CY^e class and $(33 \pm 9)\%$ for the CY^μ class, in good agreement with the above mentioned theoretical values (cf. Sect. 4.3).

4.5 Analysis of the charge asymmetry in the $l^+ \leftrightarrow l^-$ interchange

In a previous analysis [1.j] CELLO found a small indication of too large a violation of the $C_{l^+l^-}$ symmetry in the EC^l classes. We defined the asymmetry parameter $A_l = N_l^+ - N_l^-$, where $N_l^\pm$ are the fractions of the total number of observed events where both l^+ and l^- leptons satisfy $\pm q_l \cos\theta_l < 0$ in the laboratory frame. Setting $\Delta_{\text{conv}} = \Delta_{\leftrightarrow} = 1$ implies $A_l = 0$, while taking only the Δ_{conv} term into account, the expected values are close to $+1\%$. We observed a 2σ discrepancy from the above expectation in both EC^e and EC^μ classes [1.j]. A 2σ effect was also observed by the MARK J Collaboration [1.d] in a kinematical configuration similar to that of the EC^μ class. The present analysis, which is based on an integrated luminosity an order of magnitude larger, leads to values given in Table 4. The observed asymmetries are in good agreement with the QED predicitons. In particular, the value obtained in the EC^μ class is compatible with zero and does not confirm the previous indications of an abnormal violation of $C_{\mu^+\mu^-}$. A complementary analysis of EC^N events in a kinematical configuration where only one of the two muons is produced at large angle, the second escaping detection in the beam-pipe, is compatible with the hypothesis of a null asymmetry [4]. The large asymmetry observed in the EC^e class is confirmed, but is correctly accounted for by the complete formula (3) which includes the $\Delta_{\leftrightarrow}$ term.

Table 3. Sample of 4 theoretical predictions for the contributions to the total cross section of functions H_i (see text) compared to the experimental determinations given by the right-hand side of (9). The errors on the predicted values are close to 0.5%. The 16 other experimental values not presented here are in similar agreement with the corresponding QED predictions

Class	Function H_i	Observed	Predicted
FW^e	F_0	$+70.9 \pm 0.5\%$	$+70.2\%$
FW^μ	F_1	$+26.9 \pm 0.8\%$	$+28.5\%$
EC^e	$F_2 = G_1$	$-\ 1.4 \pm 0.4\%$	$-\ 2.2\%$
EC^e	G_2	$-\ 3.1 \pm 0.5\%$	$-\ 2.9\%$

Table 4. Observed and predicted asymmetries in the FW and EC classes (see text)

	Observed	Predicted
FW^e	$+\ 3.9 \pm 1.0\%$	$+2.2 \pm 0.7\%$
EC^e	$+10.2 \pm 2.0\%$	$+9.6 \pm 0.5\%$
FW^μ	$+\ 1.5 \pm 2.0\%$	$+0.8 \pm 1.0\%$
EC^μ	$-\ 1.3 \pm 2.0\%$	$+1.6 \pm 0.5\%$

However, the above defined parameter A_l is not the quantity the most sensitive to the charge asymmetry.

In order to measure the small violation of the $C_{\mu^+\mu^-}$ symmetry, we rather define

- the asymmetry function

$$A_l(k) = (M^2(k) - M_*^2(k))/(M^2(k) + M_*^2(k)),$$

where $M^2(k)(M_*^2(k))$ is the value taken by the matrix element squared for the kinematics of the k^{th} event (after the $l^+ \leftrightarrow l^-$ transformation has been applied to it),

- α_l^* the value of the parameter α which leads to the maximum of the likelihood function

$$L_l(\alpha) = \prod_{k=1}^{N} (1 + \alpha A_l(k)).$$

With *no further assumption* than that the acceptance is invariant under the $l^+ \leftrightarrow l^-$ transformation, then, irrespective of the details of the experiment, a non zero value of α_l^* establishes a violation of the symmetry $C_{l^+l^-}$, while the value $\alpha_l^* = +1$ indicates

that the symmetry is broken in precisely the expected way. Therefore, in this section of the analysis, the acceptance is extended down to smaller polar angles, where the detector response does not have a smooth behaviour. The *FW* (*EC*) tagging region now ranges from 50 (140) mrad to 80 (350) mrad. Only one of the two leptons $l^{\pm}$ is required to satisfy $|\cos\theta|<0.85$. The resulting numbers of observed events together with the corresponding expected values are given in Table 5. Combining the $ee\mu\mu$ events which belong to the three classes FW^{μ}, EC^{μ} and CY^{μ} we obtain $\alpha_{\mu}^{*}=+0.975\pm0.16$, thus establishing the $C_{\mu^+\mu^-}$ violation with a statistical significance of 6 standard deviations. A similar analysis of the *eeee* events leads to $\alpha_{e}^{*}=+1.00\pm0.05$.

5 Analysis of the double-tag events

5.1 Event selection

The selection of the double-tag events is performed in three kinematical configurations. All the selected events have been visually inspected.

5.1.a CYCY events. In this configuration, all four leptons are required to be detected within $|\cos\theta|<0.92$, the sum of their charge must be zero, and at least two of them must satisfy $|\cos\theta|<0.85$. We allow for a photon emitted at small angle ($|\cos\theta|>0.99$) if it carries less than 25% of the beam energy. There must be no isolated photon. Depending on the type of final state, the following conditions must be satisfied:

- *eeee* final state: All four combinations of particles with opposite charges must fulfill the criteria defining an electron pair.
- $ee\mu\mu$ final state: Two of the tracks must fulfill the criteria for an electron pair and the remaining two tracks for a muon pair.
- $\mu\mu\mu\mu$ final state: At least two of the tracks must be identified as muons, and all of them must be compatible with this hypothesis. All four combinations of particles with opposite charges must have an invariant mass satisfying $W>0.05$.

5.1.b CYEC events. The selection cuts differ from those applied to select the *CY* single-tag events only as far as the previously undetected positron (e^+) is concerned. Here, this particle must be isolated and satisfy $r>0.25$ and $150\text{ mrad}<\pi-\theta_{(e^+)}<350\text{ mrad}$ (or $150\text{ mrad}<\theta_{(e^+)}<350\text{ mrad}$).

5.1.c ECEC events. The selection requires the presence of a lepton pair in the range $|\cos\theta|<0.92$. At least one of these tracks must satisfy $|\cos\theta|<0.85$. In addition, two isolated *EC* tags $[e^-]$ and $[e^+]$, both with $r>0.25$, must be detected within $150\text{ mrad}<\theta_{[e^-]}<350\text{ mrad}$ and $150\text{ mrad}<\pi-\theta_{[e^+]}<350\text{ mrad}$. To reduce the background from double radia-

Table 5. Numbers of observed events in the *FW* and *EC* classes together with the corresponding QED predictions in the extended acceptance defined in Sect. 4.5

	Observed	Predicted
FW^{e}	4013	3805 ± 98
EC^{e}	1589	1640 ± 52
FW^{μ}	1393	1406 ± 47
EC^{μ}	1173	1199 ± 42

Table 6. Numbers of observed events in the double-tag configuration together with the corresponding QED predictions

	Observed			Predicted		
	CYCY	*CYEC*	*ECEC*	*CYCY*	*CYEC*	*ECEC*
eeee	16	8	21	15	11	22
$ee\mu\mu$	8	8	12	10	6.5	13.5
$\mu\mu\mu\mu$	1	[a]	[a]	0.7	[a]	[a]

[a] (not selected)

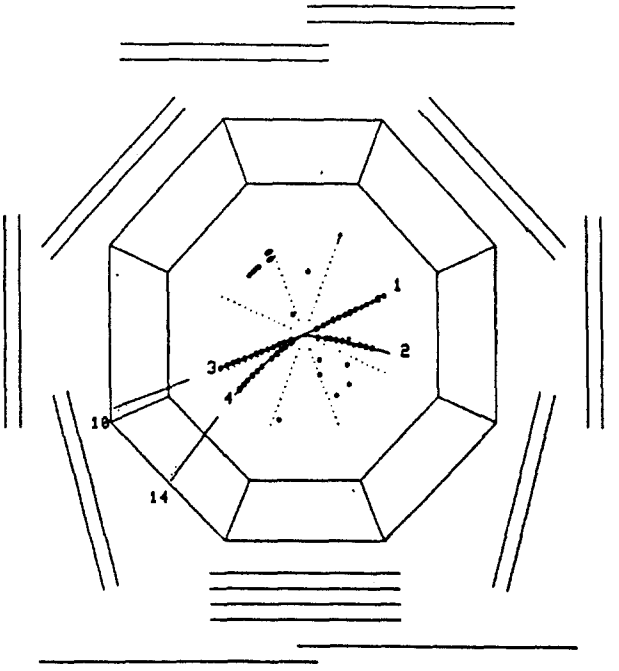

Fig. 4. The sole $e^+e^-\to\mu^+\mu^-\mu^+\mu^-$ event. The particles numbered 1, 2 and 3 are identified as muons. Particle 4 is compatible with being a muon, but has lost all its energy in the iron absorber

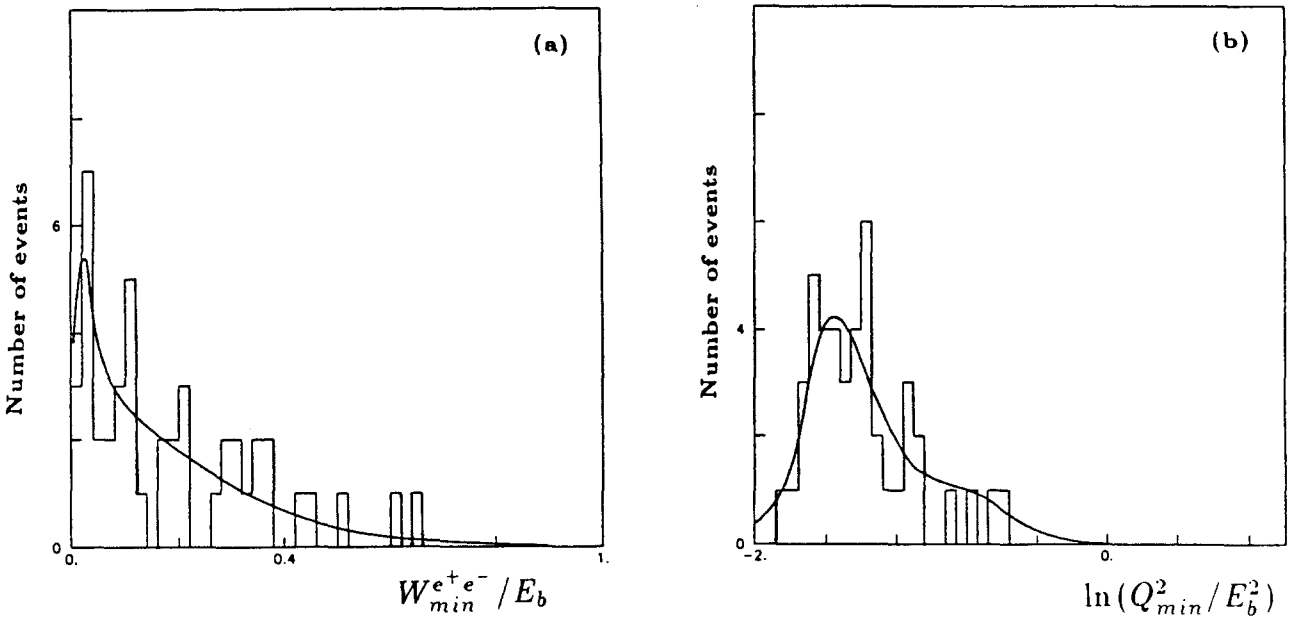

Fig. 5a, b. Distributions of the minimal e^+e^- invariant mass **a** and of the minimal momentum transfer **b** in the double-tag configuration of *eeee* events

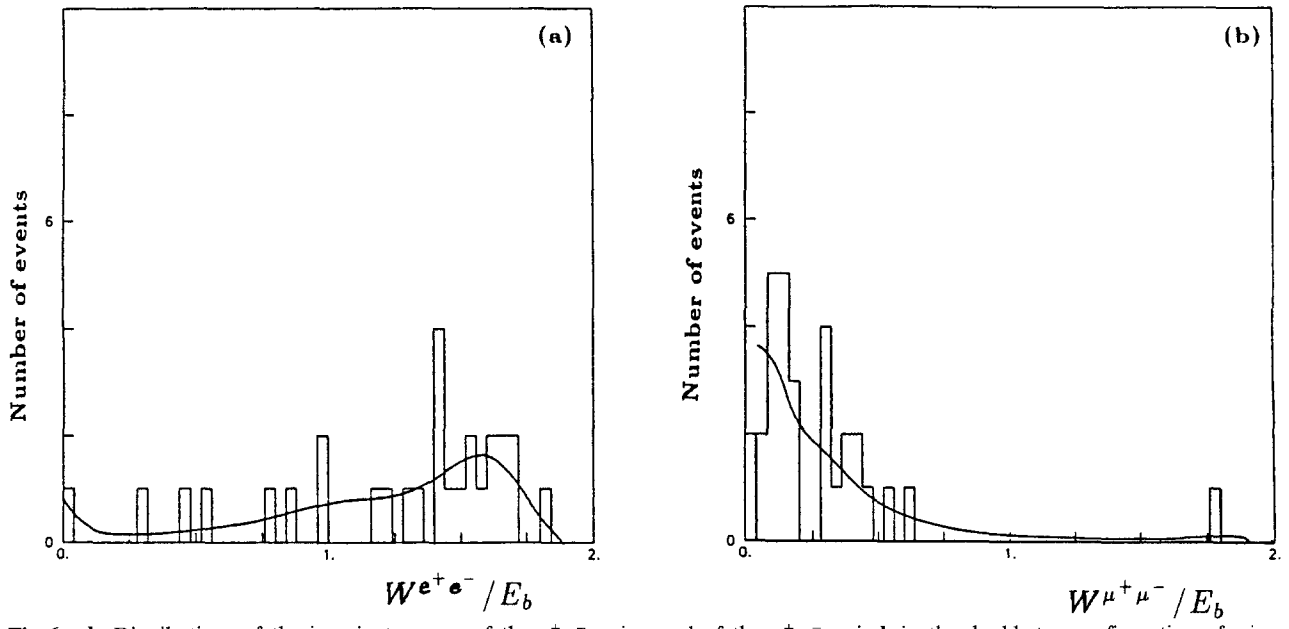

Fig. 6a, b. Distributions of the invariant masses of the e^+e^- pair **a** and of the $\mu^+\mu^-$ pair **b** in the double-tag configuration of $ee\mu\mu$ events

tive events, one of the tags must satisfy $r>0.5$ and one must be compatible with the electron hypothesis (cf. Sect. 3.3.b).

5.2 *Background*

Here again the requirements of a 'good fit' and of lepton pair identification reduce the potential sources of background to a very low level. For example, the reaction $e^+e^- \to e^+e^-\pi^+\pi^-$ could simulate the four lepton reactions if the pions were misidentified as a lepton pair. The main Feynman diagrams describing this reaction are those of the G_{conv} group where the γ_2 photon converts into a ρ. Such a background could be particularly troublesome within the acceptance defining the *CYCY* classes of *eell* events where the G_{conv}

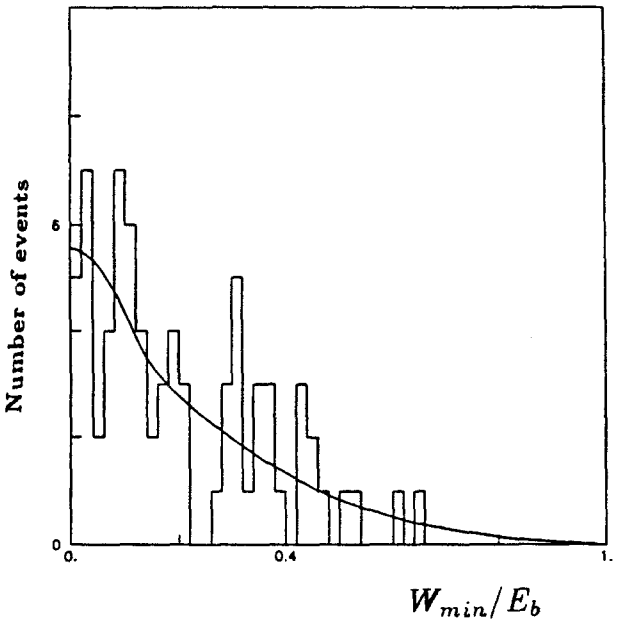

Fig. 7. Distribution of $W_{\min}$, the minimal invariant mass of lepton pairs, in the double-tag configuration (all $eeee$, $ee\mu\mu$ and $\mu\mu\mu\mu$ events combined)

group is dominant. Therefore, *CYCY* events of the type $e^+e^-\pi^\pm x^\mp$ were selected where the $\pi^\pm$ is identified on the basis of its hadronic shower development. For the 16 events observed, the distribution of the invariant mass formed by the $\pi^\pm$ and the fourth particle $x^\mp$ shows a clear peak at the ρ mass, as expected. None of the x particles of these 16 events is identified as a lepton. The background due to this reaction is estimated to be approximately one event in the case of the $eeee$ final state. It is completely negligible for the $ee\mu\mu$ and $\mu\mu\mu\mu$ final states. In a similar way, the background coming from the double radiative reactions $e^+e^-\to\gamma\gamma l^+l^-$ may affect the *ECEC* classes when one of the photons, after conversion in the beam-pipe, is mis-identified as a charged particle. From the selection of 15 $\gamma\gamma ee$ events and 1 $\gamma\gamma\mu\mu$ event in the *ECEC* configuration, this background is estimated to be less than 1 event in the $eeee$ *ECEC* class and to be negiligible in the $ee\mu\mu$ *ECEC* class.

5.3 Yields and kinematical distributions

The numbers of observed and expected events in the different classes are in good agreement (see Table 6). Altogether 74 events are observed where 79 ± 9 are expected. The one observed event with four muons in the final state is shown in Fig. 4. For the 45 $eeee$ events, the distributions of the lowest of the e^+e^- invariant masses and of the lowest of the momentum transfers Q^2 (defined in analogy with that of (2)) are shown in Fig. 5. For the 28 $ee\mu\mu$ events, the distributions of the invariant masses of the muon pair and of the electron pair are shown in Fig. 6. All these distributions are in good agreement with QED expectations. In particular, the distribution of $W_{\min}$, the minimal invariant mass of the lepton pairs, does not confirm the indication of an excess of events in the region $W_{\min}>0.4$ which was observed previously [1.c and 1.f] (Fig. 7). More generally, no indication is

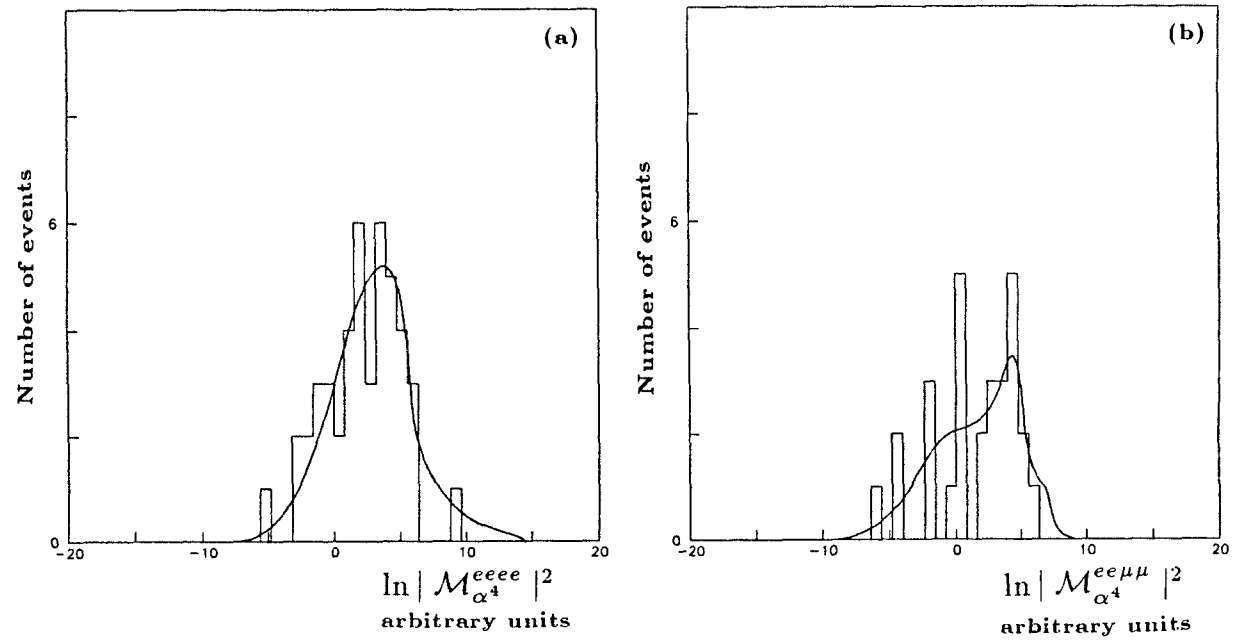

Fig. 8a, b. Distributions of the matrix element squared in the double-tag configuration for the $eeee$ events **a** and $ee\mu\mu$ events **b**

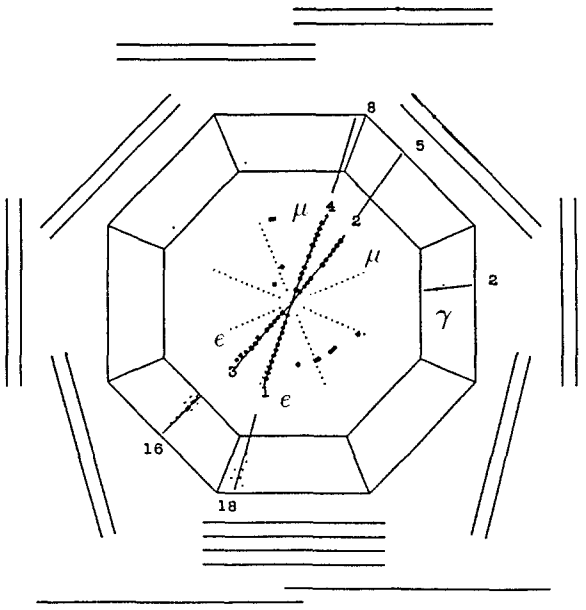

Fig. 9. One of the two $ee\mu\mu\gamma$ events observed in the $CYCY^{\gamma}$ class of double-tag events

found for an excess of events in kinematical configurations which are disfavoured by the dynamics of the QED four-lepton reactions. A signal for such an abnormal production of rare events would appear in the left side of the distributions of the matrix element squared (Fig. 8) or as an anomaly in the experimental determination of the contributions of the three groups of diagrams (see Sect. 5.4 below).

For completeness we also considered radiative events in the $CYCY$ classes. Defining the (order α^5) $CYCY^{\gamma}$ classes of events by requiring, in addition to the four leptons, an isolated photon within $|\cos\theta_{\gamma}|<0.85$, 3 events are observed: 1 $eeee\gamma$ event and 2 $ee\mu\mu\gamma$ events. Making use of the method indicated in Sect. 2.3 we expect 0.6 event: 0.36 $eeee\gamma$ event and 0.25 $ee\mu\mu\gamma$ event. Taking at face value this crude estimation, our observation would correspond to a rather low confidence level of 2.5%. One of the $ee\mu\mu\gamma$ events is presented in Fig. 9.

5.4 Determination of the contributions of the three groups of diagrams

The likelihood method used in Sect. 4.4 to analyse the multiperipheral contributions in the single-tag configuration has been used in the double-tag configuration to determine the contributions of the groups of diagrams (Fig. 1) defined in Sect. 2. The matrix element can be split in the following way:

$$\mathcal{M}_{\text{tot}}=\alpha_0\,\mathcal{M}_{\text{mul}}+\alpha_1\,\mathcal{M}_{\text{conv}}+\alpha_2\,\mathcal{M}_{\text{conv}^2},$$

where $\mathcal{M}_{\text{mul}}$, $\mathcal{M}_{\text{conv}}$ and $\mathcal{M}_{\text{conv}^2}$ are the complex matrix elements corresponding to the three groups of diagrams and where the α parameters, to be adjusted to the data, should be equal to $+1$ if the standard α^4 QED processes describe the data. Making use simultaneously of all the 74 observed events, we obtain:

$$\alpha_0=+0.94\pm0.08, \quad \alpha_1=+1.02\pm0.08$$

and

$$\alpha_2=+1.05\pm0.30,$$

in agreement with the expected values. Interferences between the different groups of diagrams make the relative signs of the three parameters measurable. The least significant sign determination is that of α_2 which corresponds to the G_{conv^2} group. Inverting the value of α_2 leads to a sizeable secondary maximum of the likelihood function, which is, however, five times smaller than the true maximum value.

6 Conclusion

We have observed the QED reactions $e^+e^-\to e^+e^-l^+l^-$ (with $l=e$ or μ) over a wide range of momentum transfer extending from the single-tag configuration at low Q^2 to the double-tag configuration at very large Q^2. In the single-tag configuration a complete expression for the differential cross section is given. The structure of the leading (multiperipheral) contribution to the cross section has been analysed and evidence has been provided for the contribution of the non-multiperipheral terms. In particular, the charge asymmetry of the cross section has been established for both $eeee$ and $ee\mu\mu$ final states. In the double-tag configuration, where, among a total of 74 events, one $e^+e^-\to\mu^+\mu^-\mu^+\mu^-$ event has been recorded, the contributions of the different groups of Feynman diagrams have been measured. Good quantitative agreement is obtained with the α^4 QED predictions.

Acknowledgements. We are indebted to the PETRA machine group and the DESY computer center for their support during the experiment. We acknowledge the invaluable efforts of all the engineers and the technicians of the collaborating institutions in the construction and maintenance of the apparatus, in particular M. Clausen, P. Röpnack and the cryogenics group. The visiting groups wish to thank the DESY directorate for the hospitality experienced at DESY. This work was partially supported by the Bundesministerium für Forschung und Technologie (Germany), the Commissariat à l'Energie Atomique and the Institut National de Physique Nucléaire et de Physique des Particules (France), the Istituto Nazionale di Fisica Nucleare (Italy), the Science and Engineering Research Council (United Kingdom), and the Ministry of Science and Development (Israel).

References

1. The most recent analyses bearing on the $ee\to eell$ reactions are: (1.a) JADE Coll. W. Bartel et al.: Z. Phys. C – Particles and Fields 30 (1986) 545; (1.b) R.P. Johnson: Ph.D. Thesis (DELCO), SLAC

Report 294 (1986); (1.c) R. Aleksan: Thèse d'Etat (CELLO), Paris VII University (1986); (1.d) MARK J Coll. B. Adeva et al.: DESY Report 85-073 (1985); (1.e) PLUTO Coll. C. Berger et al.: Z. Phys C – Particles and Fields 27 (1985) 249; (1.f) CELLO Coll. H.J. Behrend et al.: DESY Report 84-103 (1984); (1.g) PEP-9 Coll. M.P. Cain et al.: Phys. Lett. 147B (1984) 232; (1.h) MAC Coll. E. Fernandez et al.: Phys. Rev. D28 (1983) 2721; (1.i) P. Colas: Thesis (CELLO), Paris VI University (1983); (1.j) CELLO Coll. H.J. Behrend et al.: Phys. Lett. 126B (1983) 384; (1.k) The experimental situation as of 1983 is summarized by M. Pohl, Proceedings of the 5th International Workshop on Photon-Photon Collisions, Aachen (1983) 234

2. F.A. Berends et al.: Nucl. Phys. B253 (1985) 441; P.H. Daverveldt: Thesis, Leiden University (1985)
3. F.A. Berends et al.: Phys. Lett. 103B (1981) 124
4. F. Le Diberder: Thèse d'Etat (CELLO), Paris XI University, LAL Report 88-21 (1988)
5. R. Kleiss: Nucl. Phys. B241 (1984) 61
6. J. Haïssinski: LAL Report 87-11 (1987)
7. CELLO Coll. H.J. Behrend et al.: Phys. Scr. 23 (1981) 610